2018

Electron-Poor Polar Intermetallics: Complex Structures, Novel Clusters, and Intriguing Bonding with Pronounced Electron Delocalization

Qisheng Lin
Iowa State University and Ames Laboratory, qslin@ameslab.gov

Gordon J. Miller
Iowa State University and Ames Laboratory, gmiller@iastate.edu

Electron-Poor Polar Intermetallics: Complex Structures, Novel Clusters, and Intriguing Bonding with Pronounced Electron Delocalization

Abstract

Conspectus

Intermetallic compounds represent an extensive pool of candidates for energy related applications stemming from magnetic, electric, optic, caloric, and catalytic properties. The discovery of novel intermetallic compounds can enhance understanding of the chemical principles that govern structural stability and chemical bonding as well as finding new applications. Valence electron-poor polar intermetallics with valence electron concentrations (VECs) between 2.0 and 3.0 *e*–/atom show a plethora of unprecedented and fascinating structural motifs and bonding features. Therefore, establishing simple structure-bonding-property relationships is especially challenging for this compound class because commonly accepted valence electron counting rules are inappropriate.

During our efforts to find quasicrystals and crystalline approximants by valence electron tuning near 2.0 *e*–/atom, we observed that compositions close to those of quasicrystals are exceptional sources for unprecedented valence electron-poor polar intermetallics, e.g., Ca4Au10In3 containing (Au10In3) wavy layers, Li14.7Mg36.8Cu21.5Ga66 adopting a type IV clathrate framework, and Sc4Mg*x*Cu15-*x*Ga7.5 that is incommensurately modulated. In particular, exploratory syntheses of AAu3T (A = Ca, Sr, Ba and T = Ge, Sn) phases led to interesting bonding features for Au, such as columns, layers, and lonsdaleite-type tetrahedral frameworks. Overall, the breadth of Au-rich polar intermetallics originates, in part, from significant relativistics effect on the valence electrons of Au, effects which result in greater 6*s*/5d orbital mixing, a small effective metallic radius, and an enhanced Mulliken electronegativity, all leading to ultimate enhanced binding with nearly all metals including itself. Two other successful strategies to mine electron-poor polar intermetallics include lithiation and “cation-rich” phases. Along these lines, we have studied lithiated Zn-rich compounds in which structural complexity can be realized by small amounts of Li replacing Zn atoms in the parent binary compounds CaZn2, CaZn3, and CaZn5; their phase formation and bonding schemes can be rationalized by Fermi surface–Brillouin zone interactions between nearly free-electron states. “Cation-rich”, electron-poor polar intermetallics have emerged using rare earth metals as the electropositive (“cationic”) component together metal/metalloid clusters that mimic the backbones of aromatic hydrocarbon molecules, which give evidence of extensive electronic delocalization and multicenter bonding. Thus, we can identify three distinct, valence electron-poor, polar intermetallic systems that have yielded unprecedented phases adopting novel structures containing complex clusters and intriguing bonding characteristics.

In this Account, we summarize our recent specific progress in the developments of novel Au-rich BaAl4-type related structures, shown in the “gold-rich grid”, lithiation-modulated Ca–Li–Zn phases stabilized by different bonding characteristics, and rare earth-rich polar intermetallics containing unprecedented hydrocarbon-like planar Co–Ge metal clusters and pronounced delocalized multicenter bonding. We will focus mainly on novel structural motifs, bonding analyses, and the role of valence electrons for phase stability.

Disciplines

Materials Chemistry | Physical Chemistry

Electron-Poor Polar Intermetallics: Complex Structures, Novel Clusters, and Intriguing Bonding with Pronounced Electron Delocalization

Qisheng Lin and Gordon J. Miller

Ames Laboratory and Department of Chemistry, Iowa State University, Ames, Iowa, 50011

CONSPECTUS: Intermetallic compounds represent an extensive pool of candidates for energy related applications stemming from magnetic, electric, optic, caloric, and catalytic properties. The discovery of novel intermetallic compounds can enhance understanding of the chemical principles that govern structural stability and chemical bonding as well as finding new applications. Valence electron-poor polar intermetallics with valence electron concentrations (*VECs*) between 2.0 and 3.0 e^-/atom show a plethora of unprecedented and fascinating structural motifs and bonding features. Therefore, establishing simple structure-bonding-property relationships is especially challenging for this compound class because commonly accepted valence electron counting rules are inappropriate.

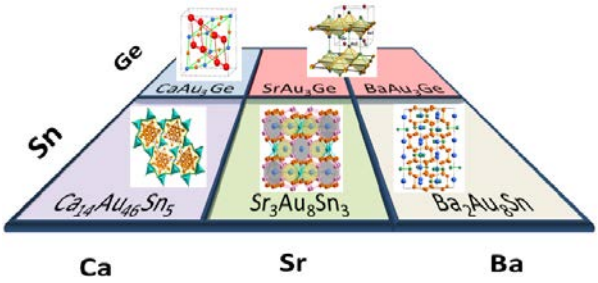

During our efforts to find quasicrystals and crystalline approximants by valence electron tuning near 2.0 e^-/atom, we observed that compositions close to those of quasicrystals are exceptional sources for unprecedented valence electron-poor polar intermetallics, e.g., $Ca_4Au_{10}In_3$ containing ($Au_{10}In_3$) wavy layers, $Li_{14.7}Mg_{36.8}Cu_{21.5}Ga_{66}$ adopting a type IV clathrate framework, and $Sc_4Mg_xCu_{15-x}Ga_{7.5}$ that is incommensurately modulated. In particular, exploratory syntheses of AAu_3T (A = Ca, Sr, Ba and T = Ge, Sn) phases led to interesting bonding features for Au, such as columns, layers, and lonsdaleite-type tetrahedral frameworks. Overall, the breadth of Au-rich polar intermetallics originates, in part, from significant relativistics effect on the valence electrons of Au, effects which result in greater 6s/5d orbital mixing, a small effective metallic radius, and an enhanced Mulliken electronegativity, all leading to ultimate enhanced binding with nearly all metals including itself. Two other successful strategies to mine electron-poor polar intermetallics include lithiation and "cation-rich" phases. Along these lines, we have studied lithiated Zn-rich compounds in which structural complexity can be realized by small amounts of Li replacing Zn atoms in the parent binary compounds $CaZn_2$, $CaZn_3$, and $CaZn_5$; their phase formation and bonding schemes can be rationalized by Fermi surface-Brillouin zone interactions between nearly-free-electron states. "Cation-rich", electron-poor polar intermetallics have emerged using rare earth metals as the electropositive ("cationic") component together metal/metalloid clusters that mimic the backbones of aromatic hydrocarbon molecules, which give evidences of extensive electronic delocalization and multicenter bonding. Thus, we can identify three distinct, valence electron-poor, polar intermetallic systems that have yielded unprecedented phases adopting novel structures containing complex clusters and intriguing bonding characteristics.

In this Account, we summarize our recent specific progress in the developments of novel Au-rich $BaAl_4$-type related structures, shown in the "gold-rich grid", lithiation-modulated Ca-Li-Zn phases stabilized by different bonding characteristics, and rare earth-rich polar intermetallics containing unprecedented hydrocarbon-like planar Co-Ge metal clusters and pronounced delocalized multicenter bonding. We will focus mainly on novel structural motifs, bonding analyses, and the role of valence electrons for phase stability.

1. BACKGROUND

Thirty-two years ago, Schäfer[1] noted "*our knowledge of the number of compounds in the (intermetallic) systems, their chemical properties, and most of important, the bonding mechanism in these phases are far less developed than in other chemical fields.*" Today, bonding characteristics of extended solids remain one of the central and challenging topics[2-7] in solid-state chemistry despite seeing rapid growth of the discovery of new intermetallic and metal-rich compounds during the past decades. Intermetallic compounds consisting of main group metals, which include groups 11 and 12 elements, can be broadly divided into three large groups according to the degree of charge transfer from electropositive to electronegative components, as sketched in Figure 1. Hume-Rothery (HR) phases[8] comprise components with similar sizes and electronegativities, so that there is minimal charge transfer and significant interatomic orbital overlap between them. HR phases occur for characteristic valence electron concentrations, or usually called (valence) electrons per atom (*e/a* values). Quasicrystals and approximants belong to HR phases, with their stability following the Fermi Surface-Brillouin Zone (FS-BZ) interaction mechanism. In contrast, the constituents of Zintl phases[9,10] have a larger electronegativity difference. Typically, the "cations" come from alkali or alkaline earth metals and "anions" are nearby the Zintl border between groups 13 and 14. Essentially complete charge

transfer between constituents is manifested in Zintl phases, thus ionic interactions contribute to bonding of the two strongly polarized counterparts, but covalent bonding exists within the anionic substructure if these atoms are not formally closed shell. The stability of anionic substructures in Zintl phases follow schemes like the Octet Rule, Wade-Mingo's Rules[11,12] and others.[13] Between Hume-Rothery and Zintl phases are polar intermetallics, which show partial charge transfer from electropositive metals (alkali, alkaline earth, or rare earth metals) to electronegative metals and/or metalloids (late transition and/or post transition elements).[9] Like Zintl phases, polar intermetallic compounds simultaneously possess ionic and covalent interactions. However, the commonly accepted valence electron counting rules fail frequently to rationalize the structures and compositions of polar intermetallics, in particular for those containing transition metals. Polar intermetallics represent a widespread pool of advanced, energy-related materials such as permanent ferromagnets, magnetocalorics, shape memory alloys, superconductors, hydrogen storage materials, and thermoelectrics. Thus, polar intermetallics have received extensive recent attention, although elucidating structure-bonding-property relationships remains challenging for these materials. Exploration of novel polar intermetallics is therefore desirable to expand the understanding of chemical principles that govern their stabilities and chemical bonding as well as to find new applications.

We began exploratory syntheses of quasicrystals and approximants ~15 years ago using valence electron tuning to the pseudogap of the electronic DOS for Mg_2Zn_{11}-type crystalline precursors.[14-20] Interested readers may refer to the review article, "A Chemical Approach to the Discovery of Quasicrystals and Approximants".[21] During the exploratory synthesis of quasicrystals, we often encountered novel complex crystalline intermetallics with compositions nearby quasicrystals, e.g., $Mg_{35}Cu_{24}Ga_{53}$,[22] $Sc_4Mg_xCu_{15-x}Ga_{7.5}$,[23] $Li_{14.7}Mg_{36.8}Cu_{21.5}Ga_{66}$,[24]

$Ca_4Au_{10}In_3$, [25] $Ca_3Au_{7.5}Ge_{3.5}$,[26] and $Ca_{14}Au_{46}Sn_5$.[27] This outcome demonstrates that a grand opportunity exists to obtain new polar intermetallics at low *e/a* values, at least for Au-based intermetallics.[28] Relatives discovered among neighboring Na/K–Au–Ga/In/Sn (A = alkali metal)[29-32] and Na/Ca/Sr/Ba-Au/Pt-Zn/Cd[33-35] systems are excellent suggestions of wonders to come in neighboring Au-rich polar intermetallic systems.

Among all polar intermetallics we have investigated, $CaAu_3Ga$ is remarkable because, as a cubic approximant with the lowest order (1/0) to an icosahedral quasicrystal,[36] this structure lacks icosahedral clusters, which contradicts the common assumption for a quasicrystal approximant. We suspect that compounds isostructural to $CaAu_3Ga$ should be prospective precursors for quasicrystals, just like Mg_2Zn_{11}-type phases. Therefore, we reinvestigated other isostructural examples, $NaAu_3Ge$ and $NaAu_3Sn$, for valence electron tuning to quasicrystals,[37,38] and designed isocompositional phases AAu_3T (A = Ca, Sr, Ba and T = Ge, Sn) for new isostructural compounds.

In this Account, we will demonstrate a profound chemistry for: (1) $BaAl_4$-type Au-rich phases by varying valence electron counts; (2) a series of novel lithiated Zn-rich intermetallics; and (3) rare earth-rich polar intermetallics containing planar hydrocarbon-like metal clusters exhibiting multicenter bonding. In all cases, the synthetic motivation, structural motifs, and phase stabilization mechanisms, such as *VEC*, size factors, and bonding features, are emphasized. Understanding the relationships among these various factors will illuminate predictable synthetic strategies of novel metal-rich compounds.

2. $BaAl_4$-Type Related Electron-Poor Au-Rich Intermetallics

According to experience,[21,28,39] gold does not behave as a noble metal in intermetallics. Au-rich intermetallics are a fertile field to discover new valence electron-poor polar intermetallics,

such as those identified in Figure 2 by loading "AAu_3T". These outcomes demonstrate that there are numerous structural motifs involving Au, and the formation and stabilization of a polar intermetallic phase is often influenced by many factors, so that any subtle change of relative atomic sizes, bond distances, valence electron counts, chemical composition, or temperature could result in a different outcome.

2.1 **$SrAu_3Ge$.** $SrAu_3Ge$ can be obtained by fusion of stoichiometric mixtures of elements at 700 ^oC for 6h, followed by slow cooling to 400 ^oC at which it is annealed for 6 days, and then quenched to room temperature. $SrAu_3Ge$ is a line compound, stable in air at room temperature. The structure of $SrAu_3Ge$ (*P*4/*nmm*; a = 6.274(1) Å, c = 5.4944(9) Å),[40] Figure 3*a*, features layers of corner-shared Au_5Ge octahedra stacked along the *c*-axis with the cavities sandwiched by uncapped Au_4 squares and filled with Sr atoms. This structure is an ordered derivative of $CeMg_2Si_2$ (*P*4/*mmm*) in which the apical atoms capping above and below the square nets are identical (Figure 3*b*). A bonding analysis of $SrAu_3Ge$ using crystal orbital Hamilton populations (COHPs) indicates that the interlayer Au–Ge contact has the largest bond population (2.96 eV/bond), followed by the apical-to-basal Au–Ge (2.35 eV/bond) and Au-Au (1.28 eV/bond) contacts, then the in-plane Au–Au (0.70 eV/bond) interaction. These values indicate that the Au_5Ge octahedra are strongly covalently bound along the *c*-direction and weaker in the *ab*-plane, and provide a rationale for the observation of "squeeze frog" like uniaxial negative thermal expansion (NTE) in *c*.[40]

$SrAu_3Ge$ is strikingly different from $ThCr_2Si_2$-type $SrAu_2Ge_2$ (*I*4/*mmm*; a = 4.519 Å, c = 10.356 Å),[40] which features layers of edged-shared square pyramids (Figure 3*c*). The different arrangements of apical atoms in these two structures reflect different bonding characteristics driven by *VEC*. $BaAl_4$-type "122" phases and its ordered variants, $ThCr_2Si_2$-, $CaBe_2Ge_2$-, and

$BaNiSn_3$-types, are optimized near 14 valence electrons per formula unit,[41] a value that can vary by $\pm 2e^-$ if the role of other factors, such as size, for structural stabilization becomes pronounced.[39] Apparently, $SrAu_3Ge$, with $9e^-$ per formula unit represents one preferred structural model for electron-poorer $BaAl_4$-related phases, as revealed by molecular orbital analyses.[40] In contrast, $CeMg_2Si_2$ is the preferred model for larger values of valence electrons per formula units ($\geq 16e^-$).[41]

2.2 $Sr_3Au_8Sn_3$. One way to circumvent a low *VEC* for a $BaAl_4$-type member is to form the La_3Al_{11}-type structure or an ordered derivative by replacing one third of the interlayer bonded atom pairs by a single atom, as observed for $Sr_3Au_8Sn_3$ (*VEC* = $8.67e^-$/"$SrAu_{2.67}Sn$"),[42] whereas $SrAu_2Sn_2$ (*VEC* = $12e^-$) adopts the $CaBe_2Ge_2$-type.[43,44] $Sr_3Au_8Sn_3$ can be obtained phase pure via stoichiometric reaction at 800 ^oC for 6h followed by annealing at different temperatures: for *T* exceeding 550 ^oC, the tetragonal La_3Al_{11}-type phase (*HT*) wins; and for *T* below 400 ^oC, the orthorhombic $Ca_3Au_8Ge_3$-type phase (*LT*) wins.[42] According to differential thermal analysis (DTA), the transition occurs at 454 ^oC. Both polymorphs feature columns of Sr-centered pentagonal and hexagonal prisms of Au and Sn stacked along the respective longest axis, see inset of Figure 4*a*. For the *HT* modification Figure 4*b*, sites shared between the different prisms are occupied by Au/Sn mixtures, whereas for the *LT* polymorph, these sites are completely ordered by one Au and one Sn atom. According to bond population analyses in Figures 4*c*–*e*, the disorder-order (*HT*-*LT*) transformation is driven mainly by covalency optimization of Au–Au and Au–Sn bonds around the Au/Sn mixed sites. The corresponding entropy change can be estimated from a standard statistical method for atomic mixing, ΔS = 2.74 cal K^{-1} mol^{-1}, and its product with the transition temperature, $T\Delta S$ = 1.99 kcal mol^{-1}, is close to that measured from DTA, ΔH = 2.54 kcal mol^{-1}.

2.3 **$BaAu_xSn_{4-x}$.** For "$BaAu_3Sn$", the product is dominated by a novel Ba_2Au_8Sn phase[45] together with minor amounts of $CaBe_2Ge_2$-type $BaAu_xSn_{4-x}$.[46] During a careful examination of the phase width of $BaAu_xSn_{4-x}$, all three ordered derivatives of the prototypic $BaAl_4$-type were found,[46] as shown in Figure 5. According to refined compositions, the homogeneity ranges for the $BaNiSn_3$-type (*I*4*mm*), $ThCr_2Si_2$-type (*I*4/*mmm*), and $CaBe_2Ge_2$-type (*P*4/*nmm*) phases are estimated to be x = 0.78(1)–1, 1.38(1)–1.47(1), and 1.52(1)–2.17(1), respectively. This outcome is meaningful for a straightforward comparison of *VEC* on the formation of $ThCr_2Si_2$-, $CaBe_2Ge_2$-, and $BaNiSn_3$-type structures. Although a few *R*-Ir-Si (*R* = rare earth) systems also contain all three structural types,[47] two "122" compositions are found as *HT* and *LT* phases with the same composition.[48] Moreover, valence electron counting for these systems is difficult arising from the unknown formal charge of Ir. Results for $BaAu_xSn_{4-x}$ reveal that the $ThCr_2Si_2$-type phase occurs at an intermediate *VEC* region of 13.6–13.8e^-/formula unit, whereas the $BaNiSn_3$- and $CaBe_2Ge_2$-type occur at higher (15.0–15.6) and lower (11.5–13.4) valence electron counts, consistent with that generalized from "coloring" of rare earth/gold/aluminum systems.[39]

Based on these results, the relationship between the formation of $BaAl_4$-type derivatives and *VEC* is clear. That is, the $BaAu_3Ge$-type/La_3Al_{11}-type, the $CaBe_2Ge_2$-type, the $ThCr_2Si_2$-type, the $BaNiSn_3$-type, and the $CeMg_2Si_2$-type structures occur sequentially from low to high *VEC* = ~8–16e^-/formula unit, or *e/a* values of 1.6–3.2. This range, in fact, covers a wide range of intermetallic compound classes from Hume-Rothery phases to Zintl phases.

2.4 $Ba_2Au_6(Au,T)_3$. The reaction targeting "$BaAu_3Sn$" also yielded the Au-richest polar intermetallic phase Ba_2Au_8Sn,[45] which was shown to be essentially a line compound formulated as $Ba_2Au_6(Au_{3-x}Sn_x)$ (x ~ 1). The structure of Ba_2Au_8Sn is rhombohedral with three independent atoms in the structure, i.e., 12*c* sites for Ba, 36*f* sites for Au, and 18*e* sites for Au/Sn mixture.

Further exploration shows that Sn in $Ba_2Au_6(Au_{3-x}Sn_x)$ can be replaced by Al, Ga, In, Zn, and Cd, with various phase widths, and the counteraction Ba can be replaced by Sr, together with possible structural distortions.[49]

The structure of Ba_2Au_8Sn is unusual in many ways. As shown in Figure 6, the structure features a hexagonal-diamond-like Au network, with voids filled by Ba atoms and $(Au/Sn)_3$ triangles in a 2:1 ratio. The formation of a diamond-like net of Au suggests significant covalent bonding, such as in the ZnS-type substructure in Heusler alloys.[50] Charge density plots confirm significantly delocalized electron density within and between the triangular units and the diamond-like Au framework, Figure 7. In fact, the structure also shows strong interactions via electron delocalization between Ba and Au atoms of the diamond-like net, as suggested by similar integrated Hamilton populations (–ICOHP values) of some Au–Au (0.60 eV/bond) and Ba–Au (0.45 eV/bond) contacts. Apparently, the chemistry and bonding of Ba_2Au_8Sn, with an exceptionally high Au content (~72.7%) or exceptionally low *e/a* value (1.45), are somewhat different from other polar intermetallic compounds due to electron delocalization.

3. Lithiated Zn-Rich intermetallics

The formation of a tetrahedral net of Au atoms in Ba_2Au_8Sn as a solution to accommodate a limited number of bonding electrons ($1.45e^-$/atom) is intriguing, as opposed to the "icosogen capability"[51] of group 13 elements to form deltahedra in response to valence electron deficiency. This outcome motivated interest to examine how group 12 elements respond in solids with low *VECs*. The Ca-Li-Zn ternary diagram serves as a good system to explore Zn-rich, yet valence electron-poor intermetallics because there is no reported ternary compound so far.

We investigated regions close to the known $CaZn_2$, $CaZn_3$, and $CaZn_5$ binaries, and found various complex structures arising from decreasing *VECs* by small additions of lithium. For

phases with *VECs* close to that of typical Zintl phases (> 3.0e^-), Zn behaves like group 13 elements by forming deltahedral clusters, e.g., icosahedra; for smaller *VECs* closer to Hume-Rothery phases (~ 2.0e^-), Zn forms heavily condensed and defect deltahedral clusters.

3.1 $Ca_{\sim 30}Li_{3+x}Zn_{60-x}$. Crystals of $Ca_{\sim 30}Li_{3+x}Zn_{60-x}$ (x = 0.44 – 1.38)[52] were obtained by reacting either $CaZn_2$ and Li in a 6:1 molar ratio or a stoichiometric mixture of Ca, Li, and Zn metals at 700 ^oC for 2h, followed by annealing at 400 ^oC for 1 week, and quenching to room temperature. The structure of $Ca_{\sim 30}Li_{3+x}Zn_{60-x}$ is hexagonal, distinctive from orthorhombic $CaZn_2$ despite only ~4 mol. % Li is added, and features a formally anionic network of interconnected Zn_3 triangles, Li-centered Zn_{12} icosahedra, and *arachno*-$(Zn,Li)_{18}$ hexagonal drums, see Figure 8. In this structure, only two out of six Zn sites mix with Li, and they are especially aggregated with the *arachno*-$(Zn,Li)_{18}$ drums. Li atoms fully occupy the site at the center of each Zn_{12} icosahedron. Since Li atoms in this structure are tightly wrapped by Zn atoms, the product is unreactive on exposure to air and water at room temperature.

The *VEC* values for $Ca_{\sim 30}Li_{3+x}Zn_{60-x}$ (~182.5e^-/formula unit) are about 10-20 electrons less than isostructural compounds $Ca_{30}Cu_{25.0}Al_{38.0}$ (199.0e^-), $Na_8K_{23}Cd_{12}In_{48}$ (199.0e^-) and $Na_{30.5}Ag_{6.4}Ga_{53.6}$ (197.7e^-). However, valence electron counting for $Ca_{\sim 30}Li_{3+x}Zn_{60-x}$ given in Table 1 yields a small difference between bonding electrons (180e^-) required for structural stabilization and the number provided from its components (~182.5e^-), suggesting that $Ca_{\sim 30}Li_{3+x}Zn_{60-x}$ is a Zintl-like compound with a small excess of valence electrons. The small discrepancy relates to the relatively large contribution of Ca–Zn polar-covalent interactions, which contribute ~41.0% toward the total bond population. In contrast, corresponding Na–Ga contributions in a hypothetical model of "$Na_{30}Ga_{60}$" based on the $Na_{30.5}Ag_{6.4}Ga_{53.6}$ structure is only 17.3%.

3.2 $Ca_{12}Li_xZn_{59-x}$ and $Ca_{15}Li_xZn_{75-x}$. Along the imaginary $CaZn_5$–"$CaLi_5$" tie-line in the Ca-Li-Zn ternary system, two novel complex structures were discovered with compositions close to $CaZn_5$. $Ca_{12}Li_xZn_{59-x}$ and $Ca_{15}Li_xZn_{75-x}$ crystallize, respectively, in rhombohedral and hexagonal space groups, with similar *a*-parameters (≈9.17 and 9.18 Å) and large *c*-parameters (≈53.60 and 45.19 Å).[53] Judging from these structural characteristics, extremely complex structures are expected for both. In fact, they belong to a large family of intergrowth structures formulated as $(A_{3m+6n})(L_{2m+3n})(M_{14})_m(M_{24})_n$, in which A and L denote formal cations and linear-chains bridging M_{14} and M_{24} clusters, as shown in Figure 9. Here M_{14} is a dimer (D) of face-sharing *hypho*-icosahedra with 14 vertices and M_{24} is a trimer (T) of a Li-centered icosahedra sandwiched by two *hypho*-icosahedra with a total of 24 vertices. Trigonal $Ca_{12}Li_xZn_{59-x}$ (m = 6, n = 3) exhibits a stacking sequence of M_{14} and M_{24} clusters as DTDDDTDDTD, whereas hexagonal $Ca_{15}Li_xZn_{75-x}$ (m = 6, n = 2) shows a stacking sequence of TDDDTDDD. Other intermetallic structural types, which are valence electron poor, also belong to this intergrowth family, including $SrMg_{5.2}$ (m = 2, n = 0), $Ba_2Li_{4.21}Al_{4.79}$ (m = 0, n = 3), and $Sr_9Li_{17.5}Al_{25.5}$ (m = 2, n = 2). In addition, Sr_8Mg_{38} and $BaLi_4$ structures are similar, but their dimers or trimers show defects or distortions.

If classical valence electron counting is applied to $Ca_{12}Li_xZn_{59-x}$ and $Ca_{15}Li_xZn_{75-x}$, there are large discrepancies between expected numbers of bonding electrons and that provided by the components ($40e^-$ versus $56e^-$). Apparently, these two phases cannot be explained by Zintl-Klemmn concepts,[54] in contrast to Zintl-like $Ca_{\sim 30}Li_{3+x}Zn_{60-x}$, because some inter- and intra-cluster bonds are omitted in the discussion of dimers and trimers of deltahedra; in particular, the intracluster bonding electrons of the concave dimer and trimer building units are not counted when applying Wade-Mingo's rules.[11,12]

Examination of *VEC* per Zn atom sheds some new light. The *VEC*/Zn for $Ca_{\sim 30}Li_{3+x}Zn_{60-x}$ is 2.90e^-, a value close to that of Zintl phases (> 3.0e^-). In contrast, $Ca_{12}Li_xZn_{59-x}$ (2.15–2.32e^-) and $Ca_{15}Li_xZn_{75-x}$ (~2.16e^-) are positioned nearer Hume-Rothery phases and *sp*-bonded close-packed metals (≤ 2e^-), a result which encouraged us to examine whether a Hume-Rothery mechanism[8] works for these two complex structures. Using the average valence electron density, the diameter of the Fermi sphere ($2k_F$) for trigonal "$Ca_{12}LiZn_{58}$" is calculated as 1.451 $Å^{-1}$, a value that closely matches 1.447 $Å^{-1}$, which is radius ($|\boldsymbol{K}_{hkl}|/2$) of the Brillouin zone defined by the (1, 2, 17) and (1, 3, 4) Miller planes, which generate the strong diffraction peak at $2\theta \approx 41.7^o$ in the X-ray diffraction pattern, Figure 10. In fact, the pseudogap in the calculated electronic DOS curve at ca. –0.5 eV corresponds to the strongest diffraction peak at ~39.5°. For hexagonal $Ca_{15}Li_xZn_{75-x}$, such calculations reveal a similar scenario, that is, the Fermi sphere is found just within a Brillouin zone defined by the (2 0 16), (2 2 0), and (3 0 10) planes, corresponding to the strongest peak at 2θ ~ 39.2°. Therefore, both $Ca_{12}Li_xZn_{59-x}$ and $Ca_{15}Li_xZn_{75-x}$ belong to Hume-Rothery phases and their phase stability can be rationalized by a Fermi surface-Brillouin zone interaction mechanism.[8]

4. Rare Earth-Rich Polar intermetallics

In previous sections, we recognized that alkaline earth metals, which are commonly assumed to be active electron donors, sometimes do not donate all valence electrons to electronegative components in valence electron-poor polar intermetallics, such as Ca in Ca-Li-Zn phases and Ba in Ba_2Au_8Sn. Rather, they exhibit pronounced covalent bonding interactions with these elements. In this section, we demonstrate that rare earth metals are also partial valence electron donors in rare earth-rich polar intermetallics.

As illustrated in Figure 11, the structure of $Pr_5Co_2Ge_3$[55] features two unprecedented molecular species, Co_2Ge_4 and $(Co_2Ge_2)_n$ with geometries resembling ethylene and polyacene, respectively. These two moieties interpenetrate planar honeycomb nets of rare earth atoms to form slabs that alternately stack with layers of rare earth tetrahedra. In comparison, the structure of $Pr_7Co_2Ge_4$ contains planar Co_4Ge_6 clusters that mimic the carbon backbone of 1,2,4,5-tetramethylbenzene. Pr atoms in $Pr_5Co_2Ge_3$ can be replaced by almost all lanthanides and Co by Ni. For $Pr_7Co_2Ge_4$, substitutions by other heavy rare earth metals for Pr and Ni for Co are also possible, with tunable dominant ferromagnetic interactions.

We suspect that these planar hydrocarbon-like metal clusters could be stabilized by specific numbers of valence electrons, like aromatic or anti-aromatic molecules. In fact, molecular orbital energy diagrams of Co_2Ge_4, $(Co_2Ge_2)_n$, and Co_4Ge_6 clusters show delocalized π and π^* bonding at the HOMO and LUMO.[55] Unfortunately, it is difficult to assign unambiguous formal charges to these metal-metalloid clusters arising from the unknown formal charge of Co and incomplete charge transfer from Pr to Co/Ge. As yet, the evidence is insufficient to conclude whether the Hückel $(4n + 2)\pi$-electron counting rule applies for aromaticity or not.

But, electron delocalization within the planar Co-Ge clusters is evident from charge density and electron localization function (ELF) plots,[55] as well as COHP plots for Co–Co and Co–Ge interactions, shown in Figure 12, which identify the states near the Fermi level to be Co–Co and Co–Ge antibonding. Onn the other hand, Pr–Co and Pr–Ge COHP curves indicate weakly bonding states at the Fermi level, which together with the Co–Co and Co–Ge COHP results suggest a delocalized bonding picture for the planar hexagonal Co-Ge cluster capped by Pr. The integrated Hamilton populations (–ICOHP values) in Table 2 indicate large polar-covalent contributions to the total bond populations arise from Pr–Co and Pr–Ge bonds, respectively,

summing to 68.6% and 71.3% for $Pr_5Co_2Ge_3$ and $Pr_7Co_2Ge_4$, and only 18.6% an d 12.6% coming from the Co-Ge clusters, although the individual Co−Co and Co−Ge bonds have the largest populations. This outcome strongly suggests significant multi-centered bonding that leads to their structural and phase stability.

5. CONCLUSION

The bonding characteristics of valence electron-poor polar intermetallics, features that are significant for cohesion and chemistry, is a debatable topic in solid-state chemistry. Factors such as *VEC*, atomic size ratios, and valence atomic orbitals are all critical for the stability of these phases, as illustrated by the Au-rich $BaAl_4$-type related compounds in Figure 2. This scenario is rather different from the dominant role of Zintl-Klemm valence electron counting rules for Zintl compounds and FS-BZ mechanism for Hume-Rothery phases.

At low *VECs*, the influence of valence electrons for metal-metal bonding from group 11 (Au) to group 12 (Zn) yields different outcomes. Au forms a stuffed, covalently-bonded hexagonal-diamond-like framework to reconcile electronic deficiency as adopted by Ba_2Au_8Sn. In contrast, Zn, with two valence electrons, forms icosahedral clusters, arising from its icosagen capability. In the case of larger *VECs*, as in $Ca_{\sim 30}Li_{3+x}Zn_{60-x}$, Zn forms interlinked networks of icosahedra, like group 13 elements; otherwise, Zn clusters must be defective or heavily condensed to avoid excessive formal negative charges, as seen in $Ca_{12}Li_xZn_{59-x}$ and $Ca_{15}Li_xZn_{75-x}$. On the other hand, rare earth rich intermetallics gain stability by significant multi-center bonding involving the rare earth metals with the electronegative components. It is apparent that many unprecedented compounds remain to be discovered.

AUTHOR INFORMATION

Corresponding Author

*qslin@ameslab.gov (Q. Lin)

*gmiller@iastate.edu (G. Miller)

Notes

The authors declare no completing financial interest.

Biographical Information

Qisheng Lin was born in Jiangxi, China. He obtained his Ph. D in 2001 from Shanghai Institute of Ceramics, Chinese Academy of Science. He carried out postdoctoral research at Ames Laboratory, Iowa State University and Rutgers University from 2001 to 2006. Afterwards, he was Assistant Scientist at Ames Laboratory before becoming a faculty member of the Department of Chemistry at University of Science and Technology of China in 2010. Currently, he holds the position of Associate Scientist at Ames Laboratory and Adjunct Assistant Professor in the Department of Chemistry at Iowa State University. He has coauthored more than 60 peer-reviewed research papers. His current research interest focuses on metal-rich polar intermetallics, magnetocaloric materials, and inorganic phosphors.

Gordon J. Miller was born in Utica, New York, USA. He received his Ph. D in Chemistry from the University of Chicago in 1986. He conducted postdoctoral research at the Max-Planck-Institute for Solid State Research from 1987 to 1990. He joined the chemistry faculty at Iowa State University in 1990, where he is currently a University Professor. He was awarded the Exxon Faculty Fellowship in Solid State Chemistry and the 2013 ACS Midwest Award. He has coauthored over 200 peer-reviewed research articles. His research group focuses on experimental and theoretical solid state chemistry, with a specific emphasis on structure-property relationships in metal-rich compounds.

ACKNOWLEDGMENT

This writing of this Account supported by the U.S. Department of Energy (DOE), Office of Science, Basic Energy Sciences, Materials Science and Engineering Division. The work was performed at Ames Laboratory, which is operated for the U.S. DOE by Iowa State University under contract # DE-AC02-07CH11358.

Table 1. Tentative Electron Counting Schemes for $Ca_{30}Li_{3+x}Zn_{60-x}$, $Ca_{12}Li_xZn_{59-}$, and $Ca_{15}Li_xZn_{75-x}$.

	$Ca_{30}Li_{3+x}Zn_{60-x}$		
	Skeleton	Exo-bond	Total
$Li@Zn_{12}$ icosahedron	$2 \times 12 + 2 = 26$	12	38
arachno-M_{18} polyhedron	$2 \times 18 + 6 = 42$	12	54
4 bonded-Zn in Zn_3	$2 \times 3 = 6$		6
Bonding electrons required		$54 \times 1 + 38 \times 3 + 6 \times 2 = 180$	
Electrons provided by components		182	
Difference / cell of $Ca_{30}Li_4Zn_{59}$		2	

	$Ca_{12}Li_xZn_{59-x}$	$Ca_{15}Li_xZn_{75-x}$
VEC of Dimer/cell	56 x 6 = 336	56 x 6 = 336
VEC of Trimer/cell	84 x 3 = 252	84 x 2 = 168
No. shared corners/cell	54	48
Charge of linear chain/cell	3 x 6+ = 18+	2 x 10+ = 20+
No. electrons required/cell	336 + 252 - 54 -18 = 516	336 + 168 - 48 -20 = 436

No. electrons provided by components/cell	395 ± 15	324
Difference / f.u.	40 ± 5	56

Table 2. Average COHP and respective contribution per cell for selected atom pairs in $Pr_5Co_2Ge_3$ and $Pr_7Co_2Ge_4$.

Bond	Distance (Å)	Ave. ICOHP (eV/bond)	Contribution (% per cell)	Bond	Distance (Å)	Ave. ICOHP (eV/bond)	Contribution (% per cell)
$Pr_5Co_2Ge_3$				$Pr_7Co_2Ge_4$			
Pr-Pr	3.545–4.060	0.34	12.8	Pr-Pr	3.448–4 .051	0.31	16.2
Pr-Co	2.924–3.044	0.87	22.3	Pr-Co	2.913–2.993	0.95	19.5
Pr-Ge	3.063–3.447	1.01	46.3	Pr-Ge	3.088–3.542	0.97	51.8
Co-Co	2.326–2.358	2.28	4.2	Co-Co	2.366	2.11	2.5
Co-Ge	2.494–2.558	1.96	14.4	Co-Ge	2.518–2.579	1.91	10.1

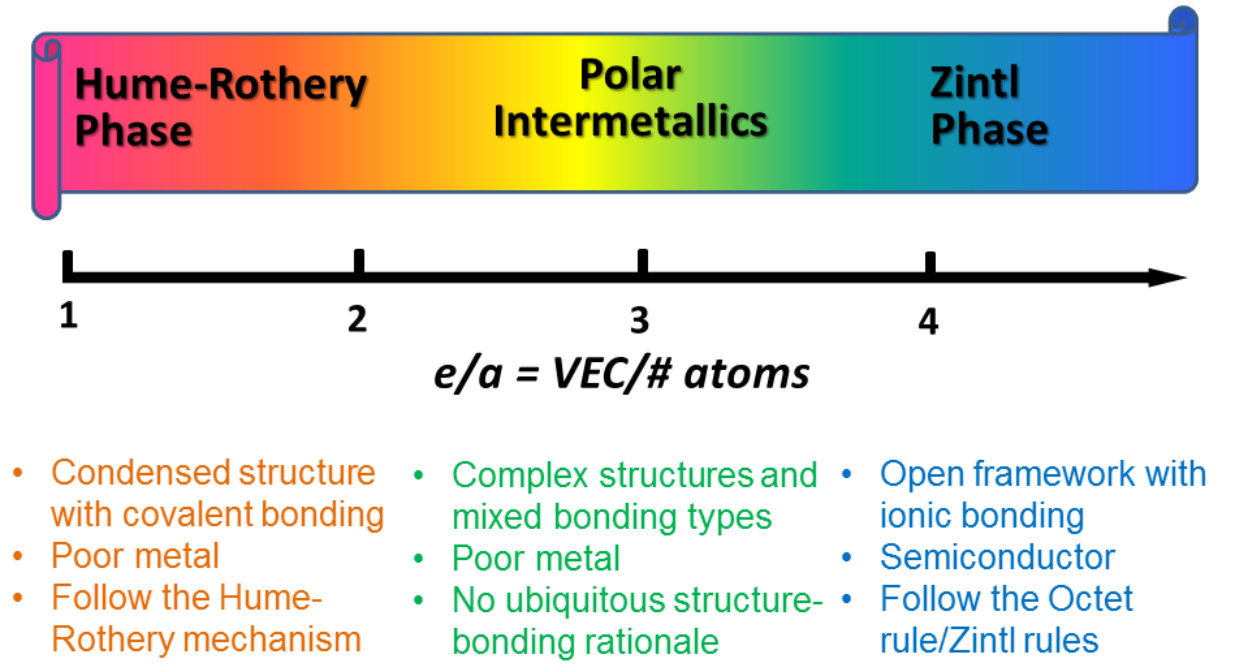

Figure 1. Relative electronic positions of Hume-Rothery phases, polar intermetallics, and Zintl phases on a scale of valence electron concentration, *e/a*.

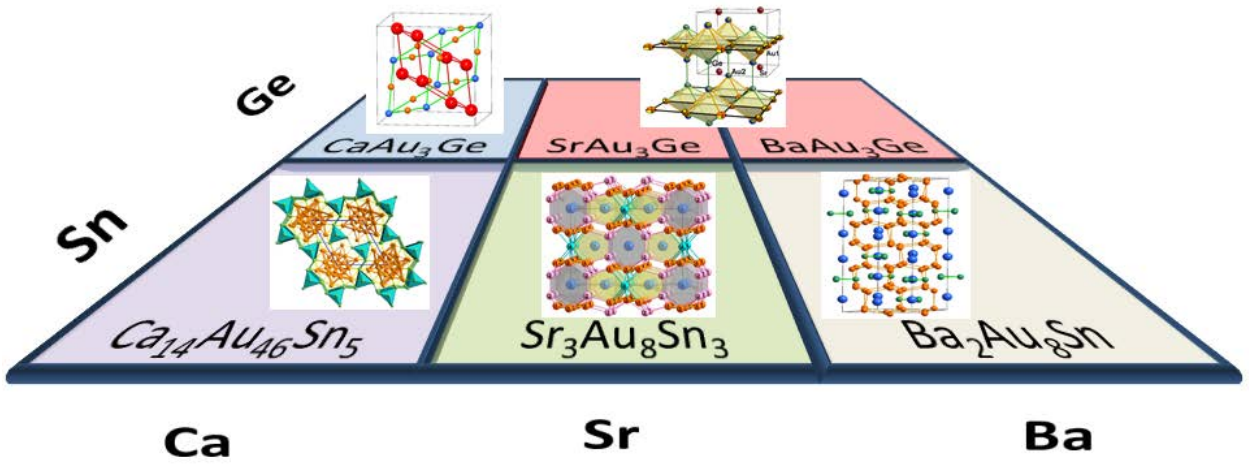

Figure 2. Various products of the 1-3-1 "gold grid" for AAu_3T (A = Ca, Sr, Ba; T = Ge, Sn).

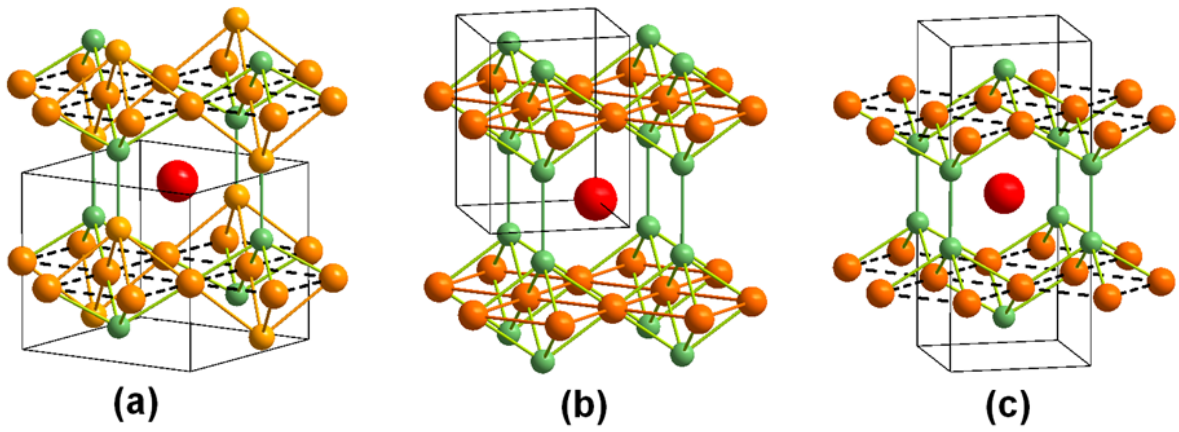

Figure 3. Comparison of crystal structures of (a) $SrAu_3Ge$, (b) $CeMg_2Si_2$, and (c) $SrAu_2Ge_2$. Red spheres represent Sr or Ce atoms, golden spheres represent Au or Mg atoms, and grass green spheres represent Si or Ge atoms. Dashed lines denote atoms are too far to be considered as bonding. (Adapted with permission from ref. 42. Copyright 2013 American Chemical Society.)

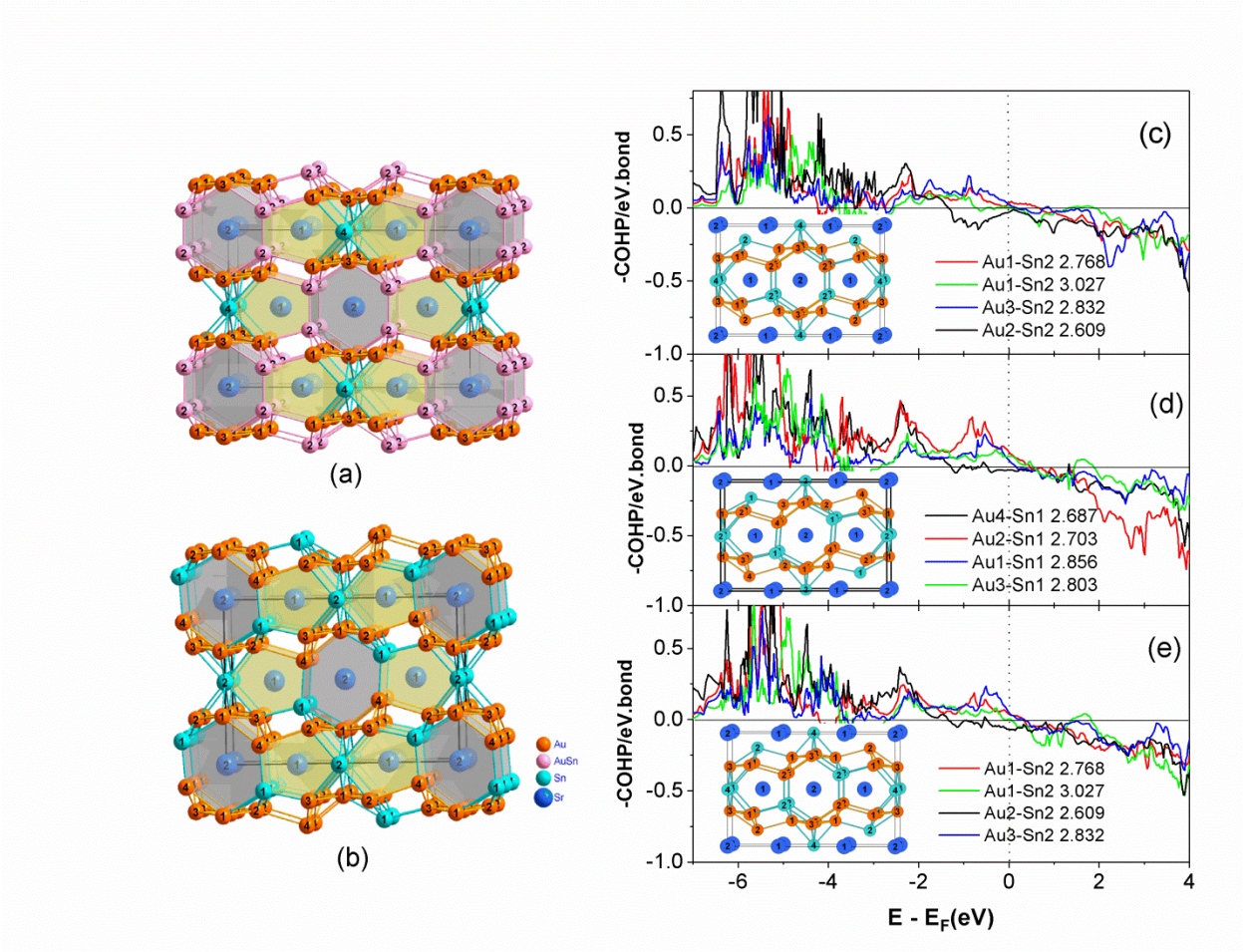

Figure 4. Crystal structures of (a) high-temperature (*HT*) and (b) low-temperature (*LT*) polymorphs of $Sr_3Au_8Sn_3$. The bond strength evaluated by –COHP data for selected Au–Au and Au–Sn pairs involved in the order-disorder transition in structural models of (c) the lowest energy model of *HT* phase, d) *LT*, and (e) pseudo-*HT* model. (Adapted with permission from ref. 42. Copyright 2013 American Chemical Society.)

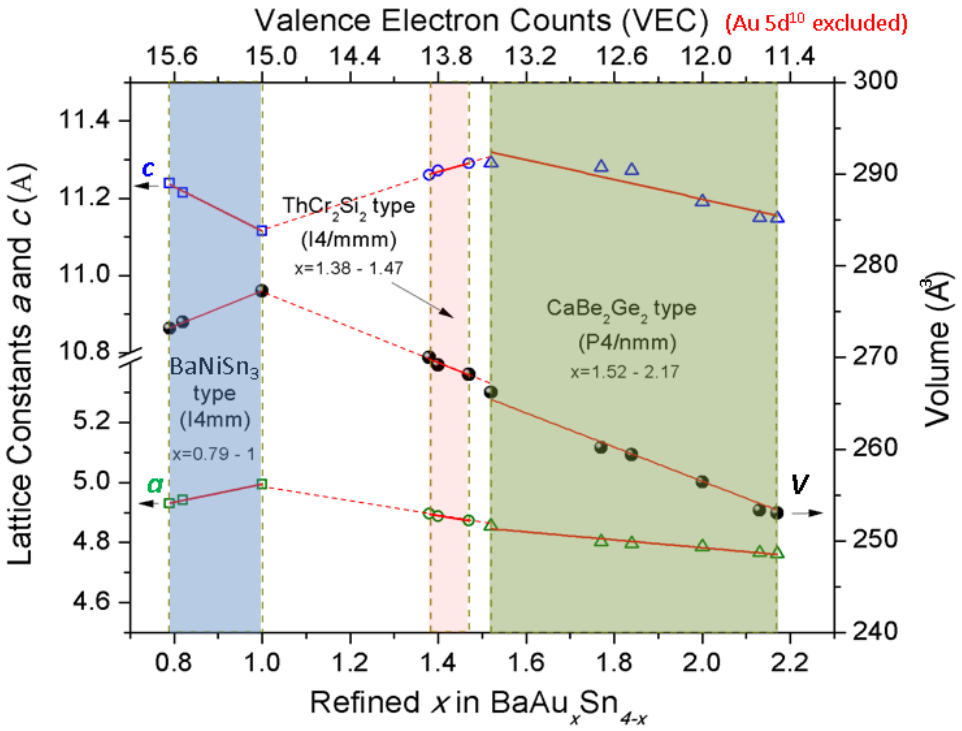

Figure 5. Relationships of lattice parameters (*a*, *c*) and unit cell volumes (*V*) versus refined *x* (bottom) or *VEC* (top) in $BaAu_xSn_{4-x}$. The different homogeneous regions are emphasized by shading. Solid (red) lines denote linear fittings in the different regions, and dashed lines, their extensions. (Adapted with permission from ref. 46. Copyright 2014 American Chemical Society.)

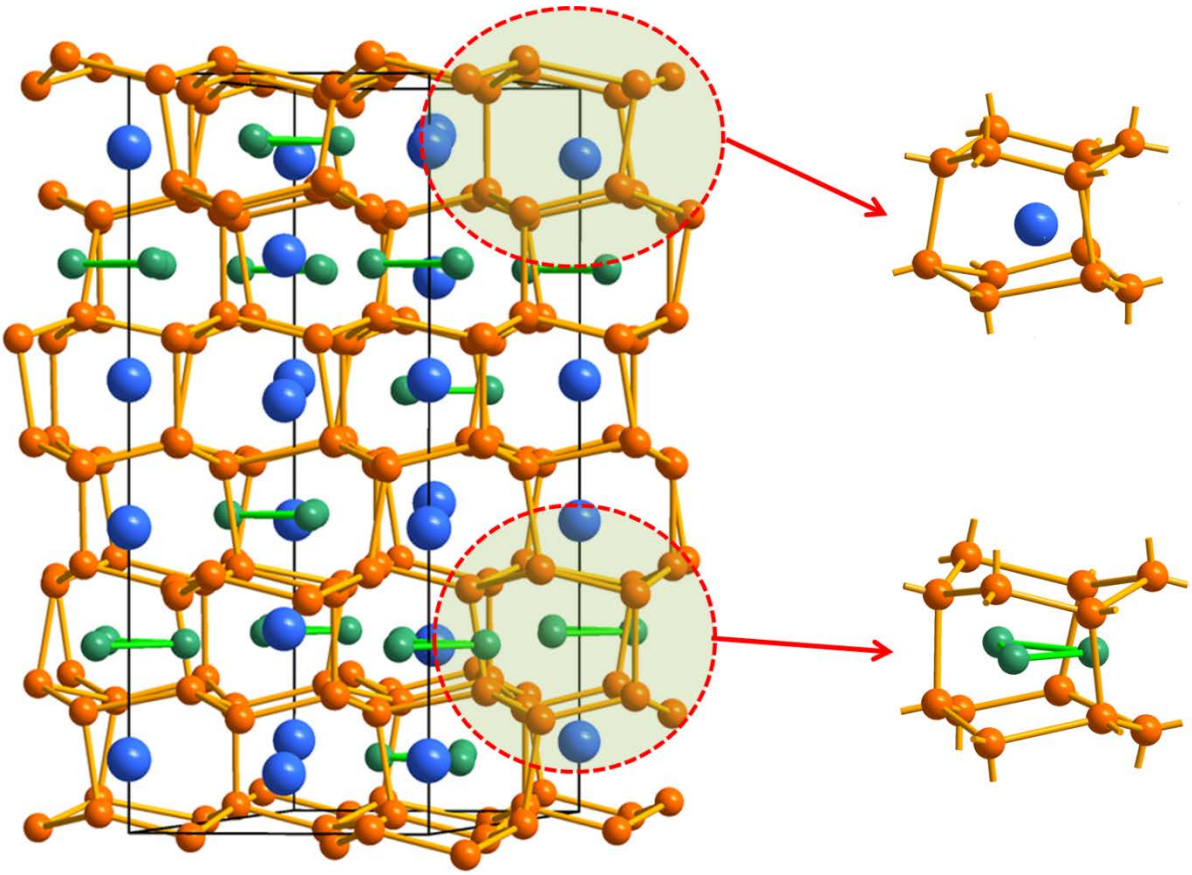

Figure 6. Crystal structure of Ba_2Au_8Sn featuring a distorted hexagonal-diamond-like Au network.

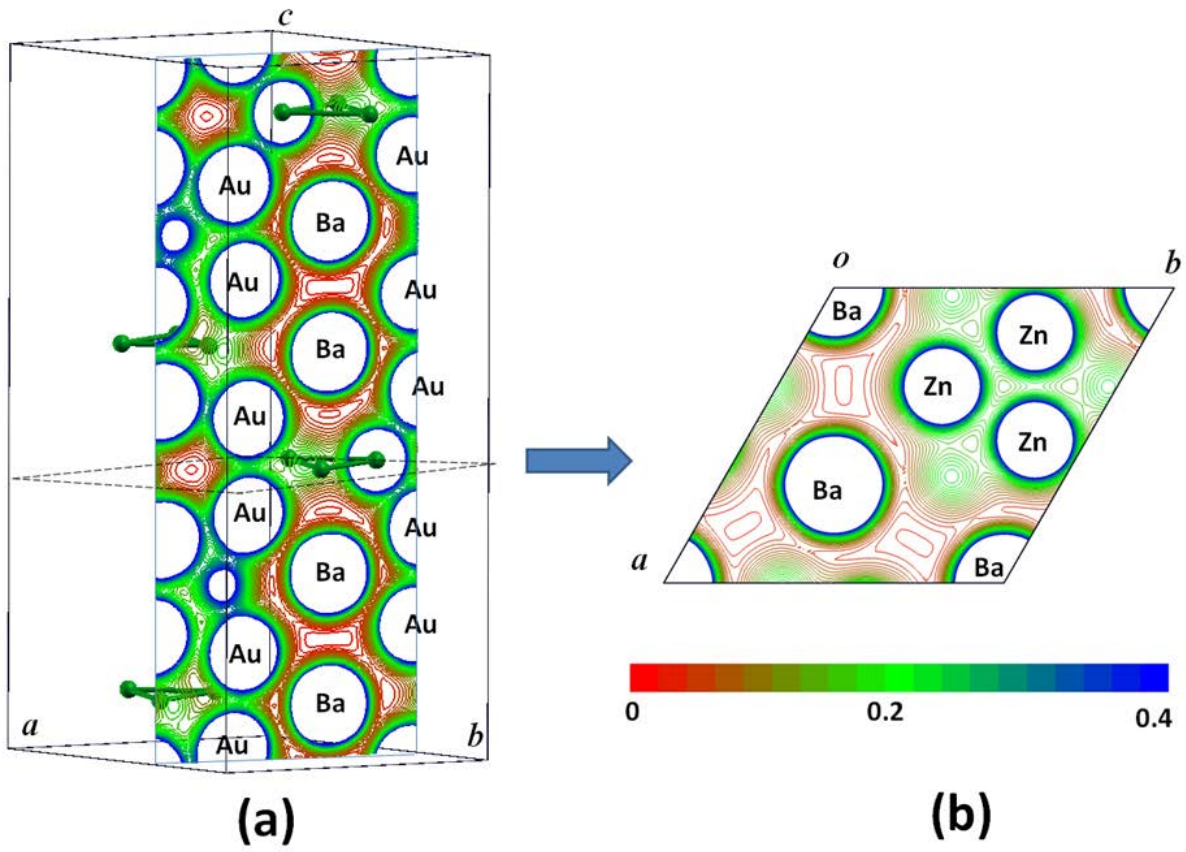

Figure 7. (a) The (110) and (b) one of selected (00z) section of charge density plots for Ba_2Au_8Sn showing electron delocalization within triangles and with Ba atoms. Note the locations of charge densities between atoms.

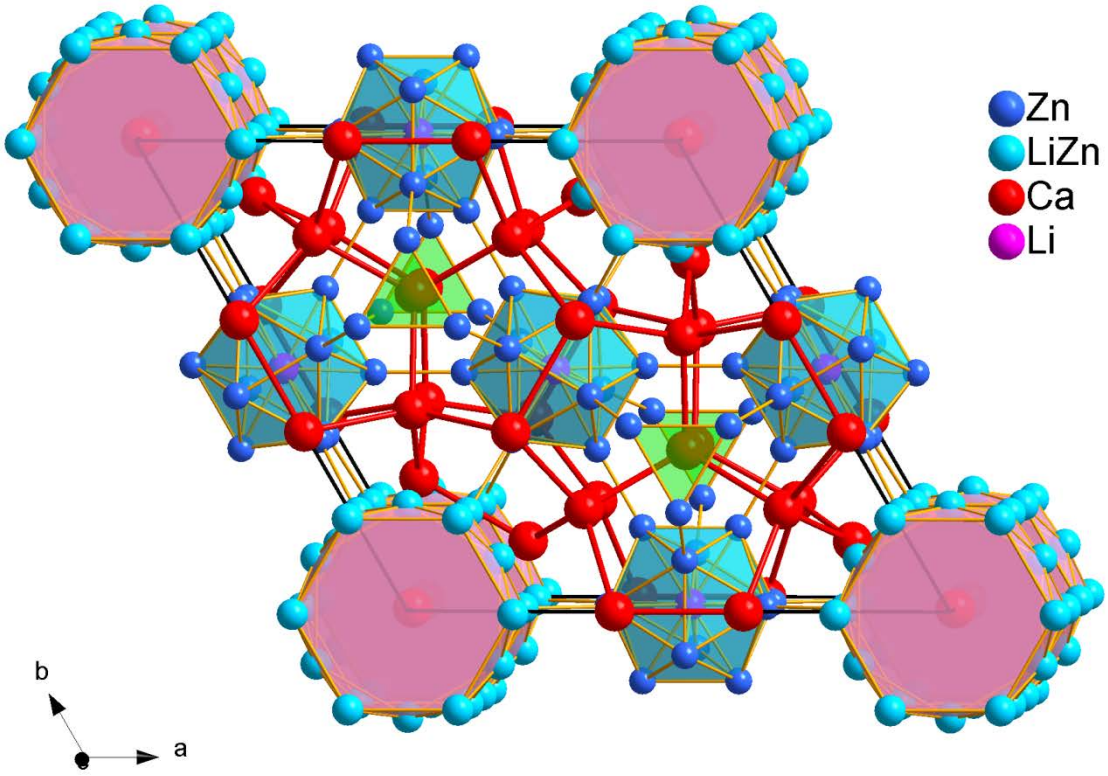

Figure 8. The structure of $Ca_{30}Li_{3+x}Zn_{60-x}$ consisting of Zn_3 triangles, Li-centered Zn_{12} icosahedra, and hexagonal $(Li,Zn)_{18}$-drums. (Adapted with permission from ref. 52. Copyright 2015 American Chemical Society.)

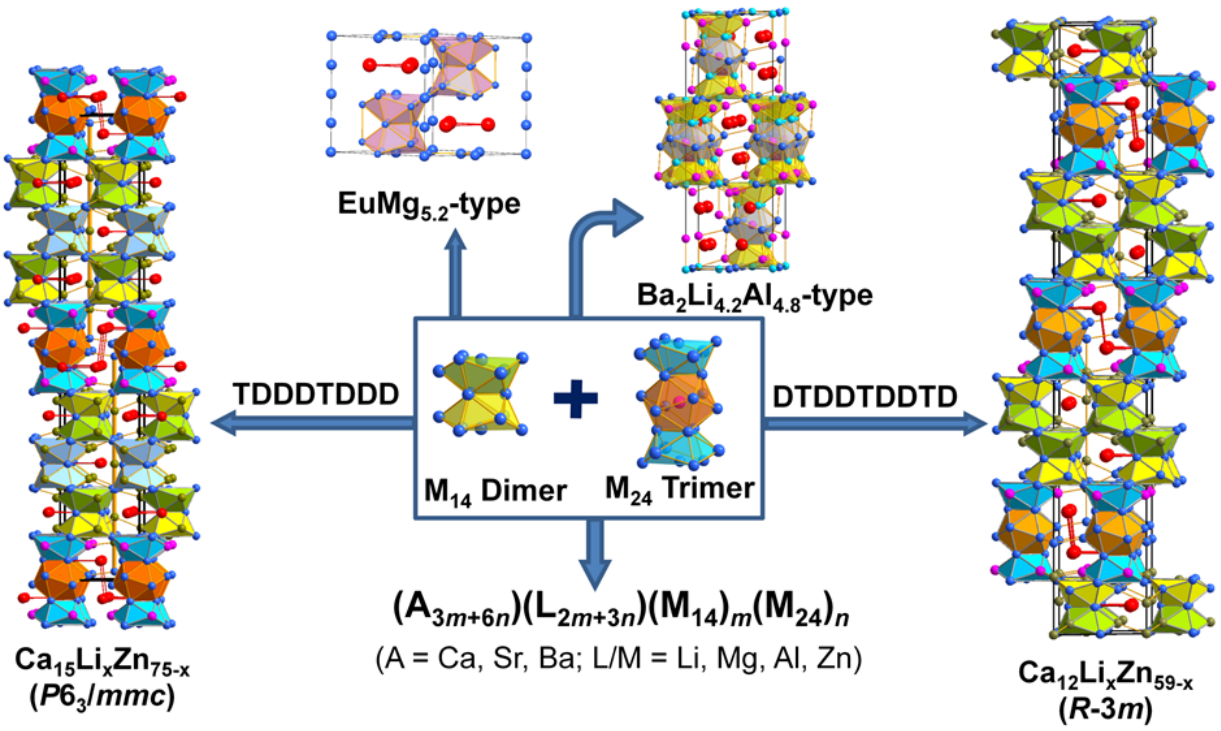

Figure 9. The intergrowth family of $(A_{3m+6n})(L_{2m+3n})(M_{14})_m(M_{24})_n$, in which A and L denote formal cations and linear-chains bridging the two complex building blocks M_{14} and M_{24} clusters shown in the middle. Two representative members, $Ca_{12}Li_xZn_{59-x}$ and $Ca_{15}Li_xZn_{75-x}$, are shown. (Reproduced with permission from ref. 53. Copyright 2016 American Chemical Society.)

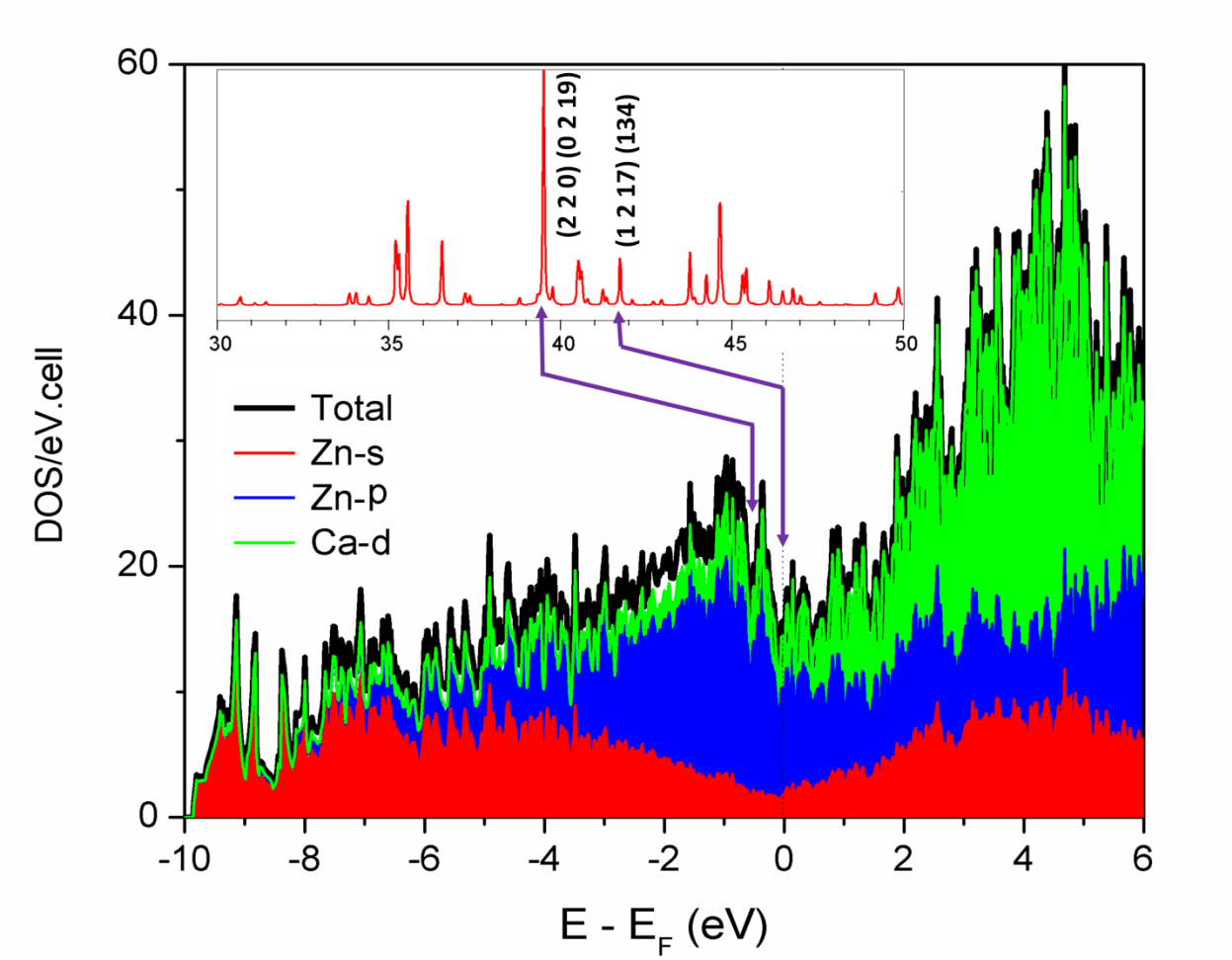

Figure 10. The electronic densityofstates (DOS) for a hypothetical trigonal "$Ca_{12}LiZn_{58}$" model. The two marked pseudogaps are generated by the two strongest diffraction peaks in a powder X-ray diffraction pattern, and fulfills the Hume-Rothery FS-BZ mechanism. (Copyright of American Chemical Society, 2016). (Reproduced with permission from ref. 56. Copyright 2016 American Chemical Society.)

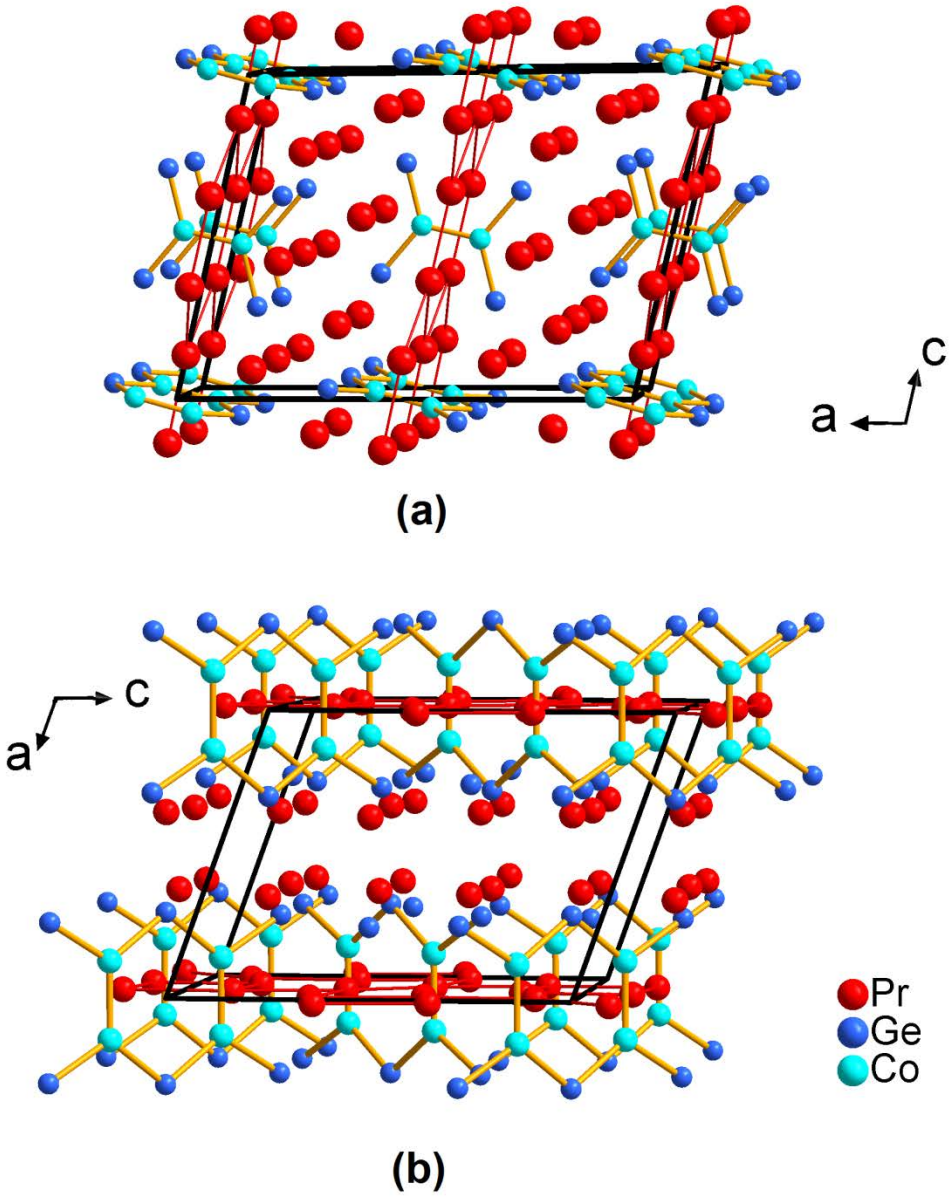

Figure 11. Crystal structures of (a) $Pr_5Co_2Ge_3$ and (b) $Pr_7Co_2Ge_4$.

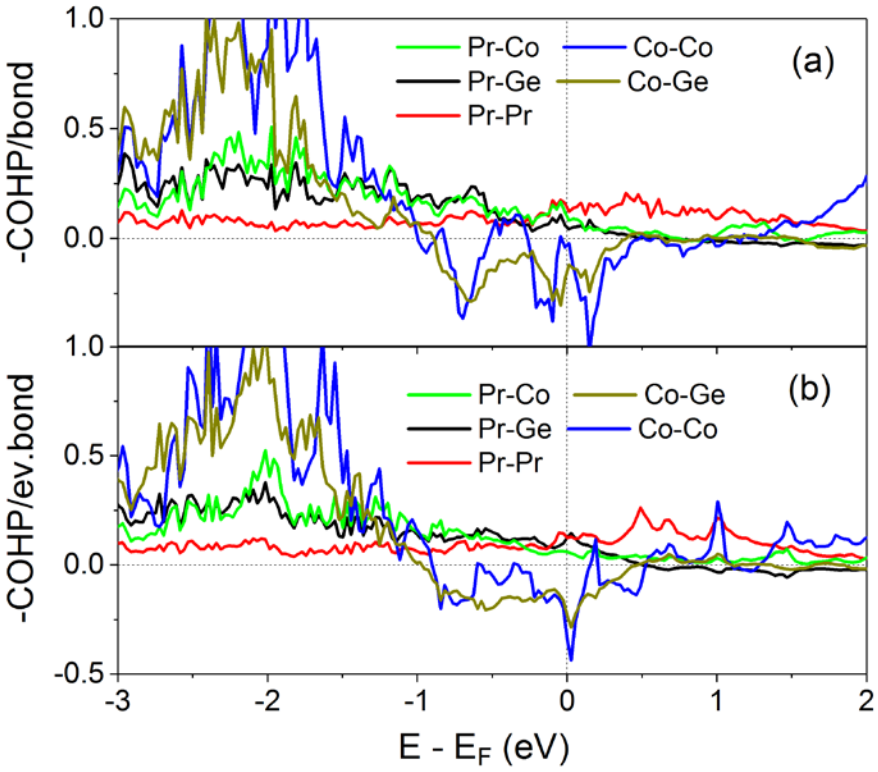

Figure 12. The COHP curves for Pr–Pr, Pr–Co/Ge, Co–Co, and Co–Ge pairs in (a) $Pr_5Co_2Ge_3$ and (b) $Pr_7Co_2Ge_4$. Note, Pr–Co and Pr–Ge curves have similar shapes and strengths around the Fermi energy; similar shapes are also observed for Co–Co and Co–Ge curves.

REFERENCES

(1) Schäfer, H. On the Problem of Polar Intermetallic Compounds: The Stimulation of E. Zintl's Work for the Modern Chemistry of Intermetallics. *Ann. Rev. Mater. Sci.* **1985**, *15*, 1-42.

(2) Tillard-Charbonnel, M.; Manteghetti, A.; Belin, C. Icosahedron Oligomerization and Condensation in Intermetallic Compounds. Bonding and Electronic Requirements. *Inorg. Chem.* **2000**, *39*, 1684-1696.

(3) Hlukhyy, V.; Eck, S.; Fässler, T. F. Localized and Delocalized Chemical Bonding in the Compounds $CaNiGe_2$, $SrNiGe_2$, and $SrNiSn_2$. *Inorg. Chem.* **2006**, *45*, 7408-7416.

(4) Simon, A. Metal clusters inside out. *Philos. Trans. R. Soc., A.* **2010**, *368*, 1285-1299.

(5) Miller, G.; Schmidt, M.; Wang, F.; You, T.-S. Quantitative Advances in the Zintl–Klemm Formalism. In *Struct. Bond*; Fässler, T. F., Ed.; Springer Berlin / Heidelberg, 2011; Vol. 139; pp 1-55.

(6) King, R. Structure and Bonding in Zintl Ions and Related Main Group Element Clusters. In *Struct. Bond*; Fässler, T. F., Ed.; Springer Berlin / Heidelberg, 2011; Vol. 140; pp 1-24.

(7) Fredrickson, D.; Doverbratt, I.; Ponou, S.; Lidin, S. Bonding Schemes for Polar Intermetallics through Molecular Orbital Models: Ca-Supported Pt–Pt Bonds in $Ca_{10}Pt_7Si_3$. *Crystals* **2013**, *3*, 504.

(8) Mizutani, U. *Hume-Rothery Rules for Structurally Complex Alloy Phases*; CRC Press: London, England, 2011.

(9) *Chemistry, Structure, and Bonding of Zintl Phases and Ions*. Kauzlarich, S. M., Ed.; VCH: New York, 1996.

(10) *Zintl Ions: Principles and Recent Developments*. Faessler, T. F., Ed.; Springer: Berlin/Heidelberg, 2011; Vol. 140, pp 156.

(11) Wade, K. Structural and bonding patterns in cluster chemistry. *Adv. Inorg. Chem. Radiochem.* **1976**, *18*, 1-66.

(12) Mingos, D. M. P. Polyhedral skeletal electron pair approach. A generalised principle for condensed polyhedra. *J. Chem. Soc., Chem. Commun.* **1983**, 706-708.

(13) Jemmis, E. D.; Balakrishnarajan, M. M.; Pancharatna, P. D. A unifying electron-counting rule for macropolyhedral boranes, metallaboranes, and metallocenes. *J. Am. Chem. Soc.* **2001**, *123*, 4313-23.

(14) Lin, Q.; Corbett, J. D. A Study of the Phase $Mg_2Cu_6Ga_5$, Isotypic with Mg_2Zn_{11}. A Route to an Icosahedral Quasicrystal Approximant. *Inorg. Chem.* **2003**, *42*, 8762-8767.

(15) Lin, Q.; Corbett, J. D. Electronic Tuning of $Mg_2Cu_6Ga_5$. A Route to Crystalline Approximant and Quasicrystalline Phases. *J. Am. Chem. Soc.* **2005**, *127*, 12786-12787.

(16) Lin, Q.; Corbett, J. D. The 1/1 and 2/1 Approximants in the Sc−Mg−Zn Quasicrystal System: Triacontahedral Clusters as Fundamental Building Blocks. *J. Am. Chem. Soc.* **2006**, *128*, 13268-13273.

(17) Lin, Q.; Corbett, J. D. Development of the Ca−Au−In Icosahedral Quasicrystal and Two Crystalline Approximants: Practice via Pseudogap Electronic Tuning. *J. Am. Chem. Soc.* **2007**, *129*, 6789-6797.

(18) Lin, Q.; Corbett, J. D. Approximant Phases and an Icosahedral Quasicrystal in the Ca−Au−Ga System: The Influence of Size of Gallium versus Indium. *Inorg. Chem.* **2008**, *47*, 7651-7659.

(19) Lin, Q.; Corbett, J. D. $M_3(Au,Ge)_{19}$ and $M_{3.25}(Au,Ge)_{18}$ (M = Ca, Yb): Distinctive Phase Separations Driven by Configurational Disorder in Cubic YCd_6-Type Derivatives. *Inorg. Chem.* **2010**, *49*, 4570-4577.

(20) Lin, Q.; Corbett, J. D. Development of an Icosahedral Quasicrystal and Two Approximants in the Ca−Au−Sn System: Syntheses and Structural Analyses. *Inorg. Chem.* **2010**, *49*, 10436-10444.

(21) Lin, Q.; Corbett, J. D. A Chemical Approach to the Discovery of Quasicrystals and Their Approximant Crystals. In *Struct. Bond.*; Wu, X.-T., Ed.; Springer Berlin / Heidelberg, 2009; Vol. 133; pp 1-39.

(22) Lin, Q.; Corbett, J. D. $Mg_{35}Cu_{24}Ga_{53}$: A three-dimensional cubic network composed of interconnected Cu_6Ga_6 icosahedra, Mg-centered Ga_{16} icosioctahedra, and a Magnesium lattice. *Inorg. Chem.* **2005**, *44*, 512-518.

(23) Lin, Q.; Lidin, S.; Corbett, J. D. Synthesis, Structure, and Bonding of $Sc_4Mg_xCu_{15-x}Ga_{7.5}$ (x = 0, 0.5). Two Incommensurately Modulated Scandium Substitution Derivatives of Cubic $Mg_2Cu_6Ga_5$. *Inorg. Chem.* **2007**, *47*, 1020-1029.

(24) Lin, Q.; Corbett, J. D. $Li_{14.7}Mg_{36.8}Cu_{21.5}Ga_{66}$: An Intermetallic Representative of a Type IV Clathrate. *Inorg. Chem.* **2008**, *47*, 10825-10831.

(25) Lin, Q.; Corbett, J. D. $Ca_4Au_{10}In_3$: Synthesis, Structure, and Bonding Analysis. The Chemical and Electronic Transformations from the Isotypic Zr_7Ni_{10} Intermetallic. *Inorg. Chem.* **2007**, *46*, 8722-8727.

(26) Lin, Q.; Corbett, J. D. Centric and Non-centric $Ca_3Au_{7.5}Ge_{3.5}$: Electron-Poor Derivatives of La_3Al_{11}. Syntheses, Structures, and Bonding Analyses. *Inorg. Chem.* **2009**, *48*, 5403-5411.

(27) Lin, Q.; Corbett, J. D. $Ca_{14}Au_{46}Sn_5$: a "Colored" $Gd_{14}Ag_{51}$-Type Structure Containing Columns of Well-Differentiated Hexagonal Gold Stars. *Inorg. Chem.* **2011**, *50*, 1808-1815.

(28) Corbett, J. D. Exploratory Synthesis: The Fascinating and Diverse Chemistry of Polar Intermetallic Phases. *Inorg. Chem.* **2010**, *49*, 13.

(29) Li, B.; Kim, S.-J.; Miller, G. J.; Corbett, J. D. Gold Tetrahedra as Building Blocks in K_3Au_5Tr (Tr = In, Tl) and Rb_2Au_3Tl and in Other Compounds: A Broad Group of Electron-Poor Intermetallic Phases. *Inorg. Chem.* **2009**, *48*, 6573-6583.

(30) Li, B.; Kim, S.-J.; Miller, G. J.; Corbett, J. D. $K_{23}Au_{12}Sn_9$—An Intermetallic Compound Containing a Large Gold−Tin Cluster: Synthesis, Structure, and Bonding. *Inorg. Chem.* **2010**, *49*, 1503-1509.

(31) Smetana, V.; Corbett, J. D.; Miller, G. J. Four Polyanionic Compounds in the K–Au–Ga System: A Case Study in Exploratory Synthesis and of the Art of Structural Analysis. *Inorg. Chem.* **2012**, *51*, 1695-1702.

(32) Smetana, V.; Miller, G. J.; Corbett, J. D. Three Alkali-Metal–Gold–Gallium Systems. Ternary Tunnel Structures and Some Problems with Poorly Ordered Cations. *Inorg. Chem.* **2012**, *51*, 7711-7721.

(33) Samal, S. L.; Corbett, J. D. Relativistic Effects and Gold Site Distributions: Synthesis, Structure, and Bonding in a Polar Intermetallic $Na_6Cd_{16}Au_7$. *Inorg. Chem.* **2011**, *50*, 7033-7039.

(34) Samal, S. L.; Lin, Q.; Corbett, J. D. Two Homologous Intermetallic Phases in the Na-Au-Zn System with Sodium Bound in Unusual Paired Sites within 1D Tunnels. *Inorg. Chem.* **2012**, *51*, 9395-402.

(35) Gulo, F.; Samal, S. L.; Corbett, J. D. Substantial Cd–Cd Bonding in Ca_6PtCd_{11}: A Condensed Intermetallic Phase Built of Pentagonal Cd_7 and Rectangular $Cd_{4/2}Pt$ Pyramids. *Inorg. Chem.* **2013**, *52*, 10112-10118.

(36) Lin, Q.; Corbett, J. D. Interpenetrating Networks of Three-Dimensional Penrose Tiles in $CaAu_3Ga$, the Structurally Simplest Cubic Approximant of an Icosahedral Quasicrystal. *Inorg. Chem.* **2008**, *47*, 3462-3464.

(37) Smetana, V.; Lin, Q.; Pratt, D. K.; Kreyssig, A.; Ramazanoglu, M.; Corbett, J. D.; Goldman, A. I.; Miller, G. J. A Sodium-Containing Quasicrystal: Using Gold To Enhance Sodium's Covalency in Intermetallic Compounds. *Angew. Chem. Int. Ed.* **2012**, *51*, 12699-12702.

(38) Lin, Q.; Smetana, V.; Miller, G. J.; Corbett, J. D. Conventional and Stuffed Bergman-Type Phases in the Na–Au–T (T = Ga, Ge, Sn) Systems: Syntheses, Structures, Coloring of Cluster Centers, and Fermi Sphere–Brillouin Zone Interactions. *Inorg. Chem.* **2012**, *51*, 8882-8889.

(39) Miller, G. J. The "Coloring Problem" in Solids: How It Affects Structure, Composition and Properties. *Eur. J. Inorg. Chem.* **1998**, 523-536.

(40) Lin, Q.; Corbett, J. D. Formation of Nets of Corner-Shared Bicapped Gold Squares in $SrAu_3Ge$: How a $BaAl_4$-Type Derivative Reconciles Fewer Valence Electrons and the Origin of Its Uniaxial Negative Thermal Expansion. *J. Am. Chem. Soc.* **2012**, *134*, 4877-4884.

(41) Zheng, C.; Hoffmann, R. D. An Unusual electron count and electron-deficient multi-center bonding in one class of intermetallics: the $BaAl_4$, $CaAl_2Zn_2$, $CeMg_2Si_2$ and FCC structures. *Z. Naturforsch.* **1986**, *41b*, 292-320.

(42) Lin, Q.; Vetter, J.; Corbett, J. D. Disorder–Order Structural Transformation in Electron-Poor $Sr_3Au_8Sn_3$ Driven by Chemical Bonding Optimization. *Inorg. Chem.* **2013**, *52*, 6603-6609.

(43) Schwickert, C.; Gerke, B.; Pöttgen, R. Gold-Tin Ordering in $SrAu_2Sn_2$ *Z. Naturforsch.* **2014**, *69b*, 767-774.

(44) Lin, Q.; Zhang, Y.; Taufour, V.; Lamichhane, T. N.; Bud'ko, S. L.; Canfield, P. C.; Dennis, K.; Miller, G. On the Structure and Stability of $BaAl_4$-Type Ordered Derivatives in the Sr-Au-Sn System for the 600 °C Section. *Z. Anorg. Allg. Chem.* **2015**, *641*, 375-382.

(45) Lin, Q.; Mishra, T.; Corbett, J. D. Hexagonal-Diamond-like Gold Lattices, Ba and $(Au,T)_3$ Interstitials, and Delocalized Bonding in a Family of Intermetallic Phases $Ba_2Au_6(Au,T)_3$ (T = Zn, Cd, Ga, In, or Sn). *J. Am. Chem. Soc.* **2013**, *135*, 11023-11031.

(46) Lin, Q.; Miller, G. J.; Corbett, J. D. Ordered $BaAl_4$-Type Variants in the $BaAu_xSn_{4-x}$ System: A Unified View on Their Phase Stabilities versus Valence Electron Counts. *Inorg. Chem.* **2014**, *53*, 5875-5877.

(47) Villars, P.; Calvert, L. D. *Pearson's Handbook of Crystallographic Data for Intermetallic Phases*; 2nd ed.; American Society of Metals: Materials Park, OH, 1991; Vol. 1.

(48) Vališka, M.; Pospíšil, J.; Prokleška, J.; Diviš, M.; Rudajevová, A.; Sechovský, V. Superconductivity in the YIr_2Si_2 and $LaIr_2Si_2$ Polymorphs. *J. Phys. Soc. Jpn* **2012**, *81*, 104715.

(49) Mishra, T.; Lin, Q.; Corbett, J. D. Gold Network Structures in Rhombohedral and Monoclinic $Sr_2Au_6(Au,T)_3$ (T = Zn, Ga). A Transition via Relaxation. *Inorg. Chem.* **2013**, *52*, 13623-13630.

(50) Graf, T.; Felser, C. Heusler Compounds at a Glance. In *Spintronics: From Materials to Devices*; Felser, C., Fecher, G. H., Eds.; Springer Netherlands: Dordrecht, 2013; pp 1-13.

(51) King, R. B. Metal cluster topology. 10. Polyhedral gallium cluster anions in intermetallic phases of gallium and alkali metals. *Inorg. Chem.* **1989**, *28*, 2796-2799.

(52) Lin, Q. Lithiation-Induced Zinc Clustering of Zn_3, Zn_{12}, and Zn_{18} Units in Zintl-Like $Ca_{\sim 30}Li_{3+x}Zn_{60-x}$ (x = 0.44–1.38). *Inorg. Chem.* **2015**, *54*, 922-929.

(53) Lin, Q.; Zhu, R.; Miller, G. J. Tuning Complexity by Lithiation: A Family of Intergrowth Structures Using Condensed hypho-Icosahedra in the Li-Doped Ca–Zn System. *Inorg. Chem.* **2016**, *55*, 5041-5050.

(54) Nesper, R. The Zintl-Klemm Concept – A Historical Survey. *Z. Anorg. Allg. Chem* **2014**, *640*, 2639-2648.

(55) Lin, Q.; Aguirre, K.; Saunders, S. M.; Hackett, T. A.; Liu, Y.; Taufour, V.; Paudyal, D.; Budko, S.; Canfield, P. C.; Miller, G. J. Polar Intermetallics $Pr_5Co_2Ge_3$ and $Pr_7Co_2Ge_4$ with Planar Hydrocarbon-Like Metal Clusters. *Chem. Eur. J.* **2017**, *23*, 10516-10521.